Physics of the Solid State, Vol. 42, No. 4, 2000, pp. 760–766. Translated from Fizika Tverdogo Tela, Vol. 42, No. 4, 2000, pp. 741–746.

LOW-DIMENSIONAL SYSTEMS AND SURFACE PHYSICS

High-Resolution Transmission and Scanning Electron Microscopy of Boride–Nitride Nanostructured Films

R. A. Andrievskiĭ[1], G. V. Kalinnikov[1], and D. V. Shtanskiĭ[2, 3]

[1]*Institute of New Chemical Problems, Russian Academy of Sciences, p/o Chernogolovka, Noginskiĭ raĭon, Moscow oblast, 142432 Russia*

[2]*Bardin Central Research Institute for the Iron and Steel Industry, Vtoraya Baumanskaya ul. 9/23, Moscow, 107005 Russia*

[3]*Department of Materials Science and Engineering, Ehime University, 3 Bunkyo-cho, Matsuyama 790-77, Japan*

Received May 12, 1999; in final form, August 6, 1999

Abstract—The results of electron-microscopic studies of grain boundaries and the structure of fractures of titanium boride- and nitride-based films obtained by nonreactive magnetron sputtering are considered. The chemical and phase composition of the films is analyzed with the help of Auger electron spectroscopy and microscopic electron diffraction analysis. The structure of boundaries and the presence of amorphous inclusions, dislocations, and other structural distortions are discussed and the nature of the deformation under indentation is considered. © *2000 MAIK "Nauka/Interperiodica".*

In the continuation of our previous research [1], it was interesting to obtain more detailed information on the structure of grain boundaries in boride–nitride films and to study the nature of their fractures. The structure of boride and nitride films has been investigated by many authors (see, for example, [2–11] and the review [12]). Some of them [4–6, 12] noted the possibility of amorphous phases forming as a result of nonequilibrium conditions of deposition. However, the data are not systematic, and the information on the type of boundaries, the presence of dislocations, and peculiarities of deformation in films based on interstitial phases is extremely scarce. This stimulated the present research using high-resolution transmission and scanning electron microscopy.

1. SAMPLES AND EXPERIMENTAL TECHNIQUE

The method of obtaining films using TiB_2–TiN targets of various compositions was described in [1]. Some of the characteristics of the investigated films deposited on silicon substrates are given in the table. The structure was studied with the help of a JEM-3010 microscope with an accelerating voltage of 300 kV. The experimental foils were prepared from films deposited on razor blades and thinned by subsequent electrolytic and ionic polishing. The crystallite size was estimated on the basis of dark- and light-field images. The phase composition was determined from x-ray diffraction and microscopic electron diffraction data. The chemical and structural composition of the films was estimated from the Auger electron spectroscopic data (obtained on a Varian Scanning Auger electron spectrometer).

The microhardness of the films on silicon substrates was measured by the Vickers hardness test on a PMT-3 instrument using loads of 0.2–0.3 N; on the basis of 5–7 measurements, the value of H_0 corresponding to the hardness of films proper was estimated by the method [13] that makes it possible to eliminate the

Characteristics of investigated films

Film type	Sputtering regime (target)	Thickness, μm	Structural type	Lattice parameters, nm		Crystallite size, nm	Hardness H_V, GPa, under load P, N		H_0, GPa	Composition
				a	c		0.2	0.3		
I	DC(TiB_2)	1	AlB_2	Unknown		2–5	34	24	70–80	Unknown
II	HF(TiB_2)	1.7	AlB_2	0.3048	0.318	3–5	31	21.5	40–49	$Ti(B_{0.92}O_{0.05}C_{0.03})_{1.61}$
III	HF(50TiB_2–50TiN)	0.4	NaCl	~0.428		0.5–3	26	21	47–54	$Ti(B_{0.34}N_{0.49}O_{0.12}C_{0.05})_{1.49}$
IV	HF(25TiB_2–75TiN)	1.3	NaCl	~0.4307		5–15	23	19	42–43	Unknown

Note: DC indicates sputtering under direct current conditions and HF is the high-frequency mode.

1063-7834/00/4204-0760$20.00 © 2000 MAIK "Nauka/Interperiodica"

effect of the substrate and film thickness on the results of measurements.

Fractographic measurements were made on a scanning microscope Hitachi S-4000 using a technique [3, 8] allowing one to observe the behavior of the material at the center of deformation. In other words, we studied the surface of cracks passing through pricks appearing as a result of microindentation (under loads of 1–5 N).

Preliminary results concerning the structure and fractography of films I and IV (see table) were reported in [8, 14].

2. DISCUSSION OF RESULTS

2.1. Structure and Composition

Figure 1 shows some dark-field images of films that visually indicate the presence of a nanocrystalline structure with a crystallite size generally smaller than 5–15 nm (films I, II, and IV). Especially small grains are observed for films III, deposited by sputtering from targets of an equimolar composition and having the smallest thickness.

Figure 2 illustrates several microscopic electron diffraction patterns of the synthesized films. The electron diffraction pattern obtained from one of the largest crystallites of film IV (Fig. 2c) confirms the presence of a structure of the NaCl type. The values of lattice parameters presented in the table were calculated predominantly from microscopic diffraction data, and, hence, their accuracy is not high. In our earlier publication [1], we discussed the difference between the lattice parameters and the tabulated data, which is due to the composition and the presence of a large number of impurities, as well as to deformation-induced displacements of diffraction maxima. According to Deng *et al.* [5], considerable compressive residual stresses can be expected in nitride–boride films.

A general analysis of x-ray and microscopic electron diffraction patterns also leads to the conclusion that, in view of the absence of a visible halo, amorphous phases are either absent or scarce.

According to the results of the Auger analysis, the distribution of elements over the film thickness was quite uniform except in a thin surface layer ($\delta \sim 30$ nm). It should be noted that these data correlate well with our previous results [1] and confirm the formation of a prestoichiometric phase on the basis of titanium diboride and a superstoichiometric phase on the basis of titanium nitride. As before [1], while writing the structural composition, we presumed that the film structure contains only one phase (judging from x-ray and electron diffraction patterns), and all interstitial atoms are in the nonmetallic sublattice.

We did not observe any difference in the phase composition and structure between the films deposited on silicon and steel substrates.

2.2. High Resolution

Figure 3 shows some photographs obtained in the direct resolution mode. It can be seen that, in contrast to noncrystalline materials prepared by consolidating ultrafine powders and normally characterized by a certain number of residual pores [15], film-type nanostructured objects are virtually free of pores. It can also be observed that the overwhelming number of grains have a stripe structure typical of the crystalline state, although individual regions could be characterized as amorphous. One such region denoted by A is shown in Fig. 3c. The number of regions with a blurred image, a violation of the stripe structure, and an indication of "amorphism" becomes so significant in the structure of film III (Fig. 3e) that it creates the impression that crystalline grains of size 0.5–2 nm are located in an amorphous matrix. It should be noted that the number of NaCl unit cells ($a \sim 0.43$ nm) in a crystallite having a size ~1 nm is just eight, and according to simple estimates, the fraction of boundary regions for crystallites

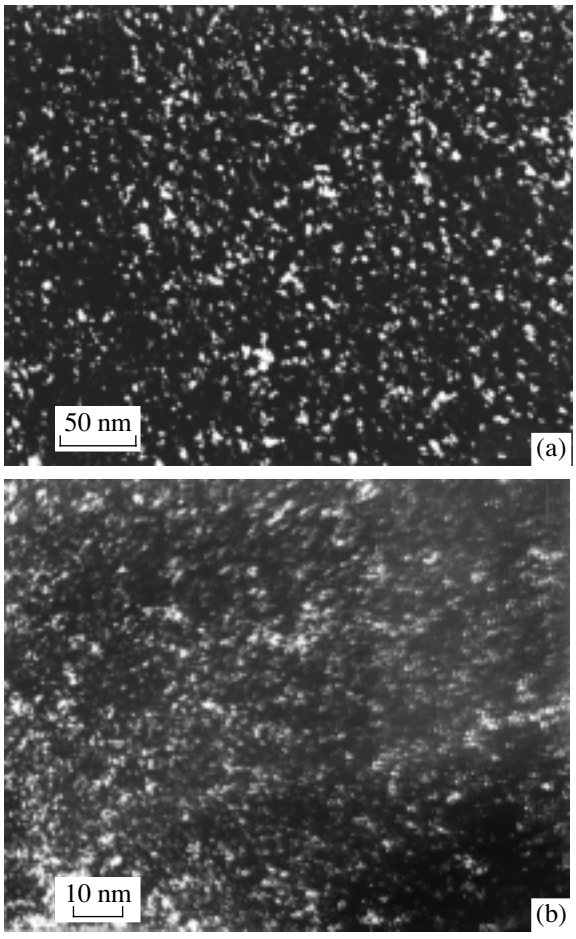

Fig. 1. Dark-field electron micrographs: (a) film I and (b) III.

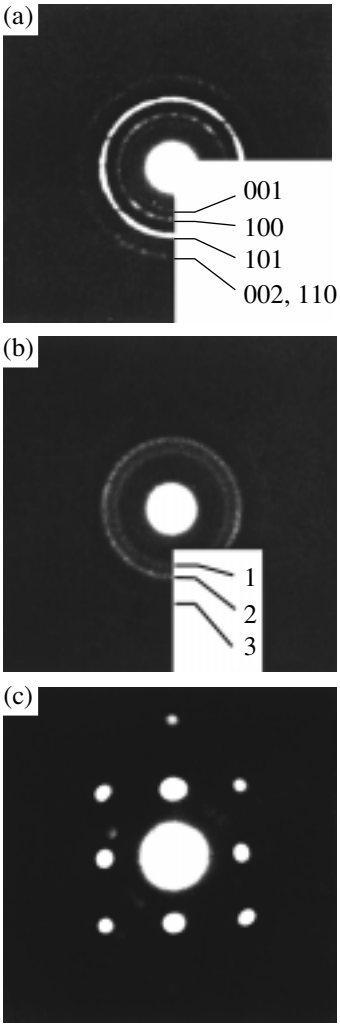

Fig. 2. Microscopic electron diffraction patterns: (a) film II, (b) III, and (c) IV (single crystal, axis [001]).

of this size can be 50%, and even higher for a boundary width ~0.3 nm. In the case of film III, whose image differs in general from those of other films, we are actually dealing with a sort of crystallite-like clusters displaying considerable structural distortions, which was also detected from displacements of diffraction lines.

In all probability, the "amorphous" nature of some other regions is associated with the effect produced on the image by numerous boundaries between crystallites, which are not parallel to the electron beam, and by above-mentioned possible internal stresses in the films. Besides, the blurring of images is also quite likely for crystallites having a size < 5 nm, whose number over the thickness of a foil under investigation (normally close to 5 nm) can be two or more, so that the interpretation of the presence or absence of amorphous inclusions becomes quite problematic. This looks significant for films I–III (especially for film III) with fine crystallites dominating in the structure (see table). Thus, the absence of amorphous inclusions in films IV, as well as in films I and II to a considerable extent, appears quite probable, while the situation with the object having finest grains (film III) is unclear on account of the large fraction of boundary regions, although the absence of a visual halo on x-ray and electron diffraction patterns was noted for all types of the films under investigation (see above).

In Figs. 3a and 3c, the boundaries between grains, at which the crystalline structure of both grains is seen more or less clearly, can be observed in many regions; atomic stripes terminate at the boundaries whose structure is of the crystalline form (arrows in Fig. 3c). The width of large-angle boundaries constitutes ~0.5 nm or even less. In some cases, the presence of coherent boundaries was detected.

Figure 3d shows, under a large magnification, the lower right corner of the image of film IV depicted in Fig. 3c, where there is a large grain approximately 20 nm in diameter. The clearly manifested inhomogeneous contrast (the focusing varied over distances shorter than 5 nm) can be attributed to internal stresses and the difference in composition, but the latter is unlikely.

Finally, an important point in observing direct-resolution structures is the detection of dislocations and other structure distortions. Bending of stripes in stripe patterns is noticeable in many cases (see, for example, Fig. 3a). We can also distinguish several edge dislocations, which are also seen clearly in the limits of the large nanocrystal in film IV (see Fig. 3d). In the structure of hexagonal films (Figs. 3a and 3b), dislocations are observed less frequently and are mainly located near boundaries.

It is well known [16, 17] that the presence and motion of dislocations in small crystalline objects is limited not only by frictional forces of the lattice (Peierls–Nabarro stress σ_{PN}), but also to a considerable extent by the so-called image forces emerging at interfaces and determining the stability of dislocations. The estimates obtained by Gryaznov *et al.* [17] for a number of metallic nanocrystals (Cu, Al, Ni, and Fe) indicate that the characteristic linear size for these materials, below which the existence of edge dislocations is highly improbable, is 2–24 nm. Unfortunately, the information on σ_{PN} for the refractory compounds under investigation is extremely scarce. If we use the estimate of the critical shear stress for TiN (σ_{cr} = 3.7 GPa) [18] and assume, as is usually done for refractory compounds [19], that $\sigma_{PN} \sim \sigma_{cr}$), then from the expression $\Lambda = 0.04Gb/\sigma_{PN}$ [17], where G is the shear modulus (248 GPa [1, 19]) and b is the Burgers vector (0.298 nm), we obtain the characteristic linear size, $\Lambda \sim$ 0.8 nm, below which the probability of existence of edge dislocations in nanocrystals is very low. This value is in satisfactory agreement with our experimental results. The approximate nature of the estimates for

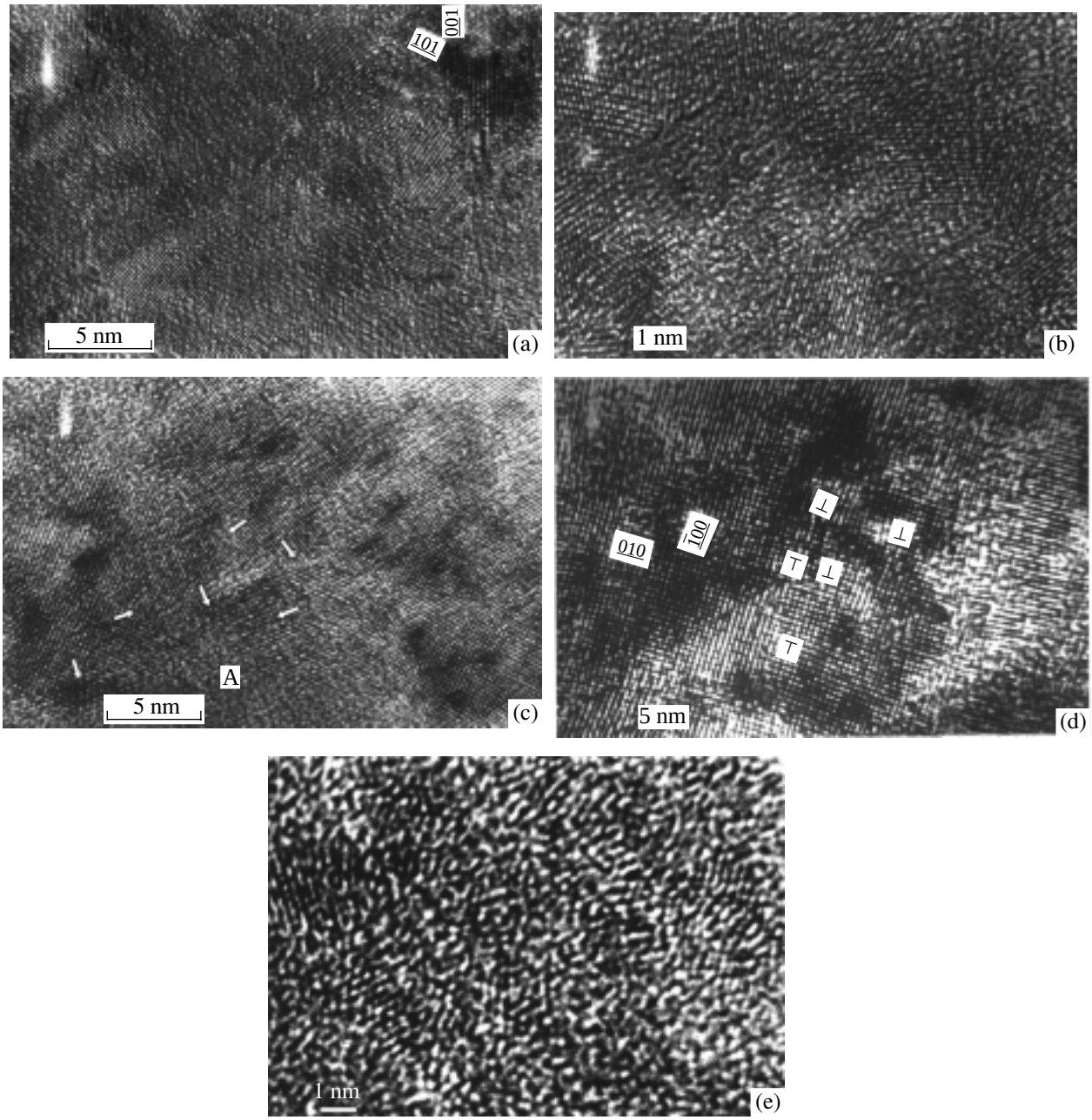

Fig. 3. Photographs of a film structure made in direct resolution mode: (a) film I, (b) II, (c) IV, (d) IV (one crystallite), and (e) III.

Λ does not allow us, however, to find the difference between phases based on TiN and TiB_2 nanocrystals.

2.3. Fractography

Figure 4 shows characteristic fractures of films with a cubic (a–c) and a hexagonal (d, e) structure. Judging from the plane of imprint and fracture, the deformation in the former case is more or less homogeneous, while in the latter case the step formation and localization of shear strains in the direction of force exerted by an indentor are quite obvious, and the deformation appears to be nonhomogeneous. When large loads (>1 N) are applied during indentation, annular and radial cracks are formed at the imprint surfaces in the case of cubic films (see Fig. 4b), as is usually observed in the case of hardness measurements in brittle solids, but no shear steps were observed in the load range under investigation (up to 5 N). An analysis of fractures of hexagonal films shows that the height and width of steps vary from ~100 nm to several hundred nanometers.

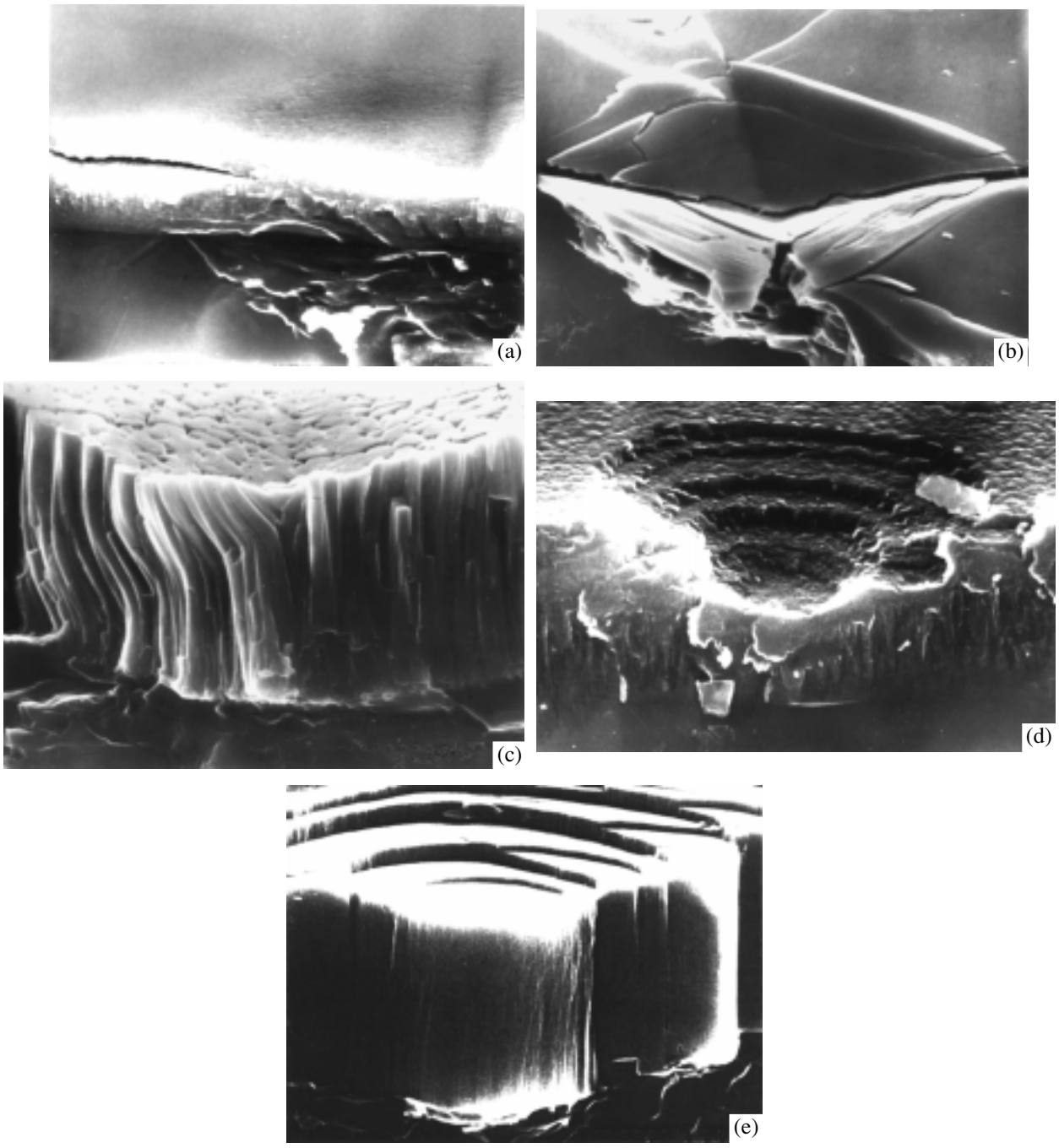

Fig. 4. Fractographs of fractures in (a–c) TiN-based films with a cubic structure and (d, e) TiB_2-based films with a hexagonal structure. (Courtesy of K.Y. Ma and A. Bloyce [27].)

Localized nonhomogeneous deformation is known to occur in many types of solids: metallic glasses, metals and alloys (including single crystals), ionic crystals, polymers, etc. The nature of this phenomenon is being discussed widely, although no satisfactory explanation of this effect have been obtained as yet (see, for example, [20–23]). On the other hand, in recent publications concerning the deformation of nanostructured materials (prepared from ultrafine powders of Fe, Fe–Cu, and $ZrO_2 + 3\%Y_2O_3$), the step formation and localization of shear strains were also reported [24–26]. In this connection, the nonhomogeneous deformation we detected for the first time [8] in nanostructured TiB_2-based films with a hexagonal structure is not surprising. However, it is not clear why TiN-base nanostructured films with a cubic structure are deformed homogeneously, which

can also be confirmed by an analysis of the fractures of this type of films in [3, 8, 27]. It was proposed [14, 28] that this is due to different numbers of independent slip systems in TiB_2 (two systems of the type $\{10\bar{1}0\}\langle 11\bar{2}0\rangle$) and in TiN (five systems of the type $\{111\}\langle 110\rangle$). However, recently information on the behavior of dislocations in monocrystalline films and polycrystalline compacts of TiN [18, 29] convincingly proves the preferred slip along the {110}-type planes in the same direction ⟨110⟩ (the number of independent slip systems is also two in this case).

Peculiarities of the deformation of cubic and hexagonal boride–nitride films can also be attributed hypothetically to the difference in the behavior of boundaries between columns in these films. In the former case, a clearly manifested columnar structure is observed as a rule (see Fig. 4c), and a uniform slip along columns under the action of the indentor is obvious. In the latter case, the columnar structure is less pronounced (see Fig. 4d), and deformation is localized through step formation, although the mechanism of this phenomenon (as for other objects listed above [20–26]) remains unclear and requires further investigations.

It is important to note that the objects under investigation are brittle by nature and are characterized by intercrystallite fracture [28]. Nevertheless, the presence of intracrystallite dislocations noted above (see Fig. 3d) facilitates the manifestation of plastic deformation, a unique example of which is depicted in Fig. 4c. The residual deformation of a part of "columns" in brittle TiN after indentation can be seen clearly; hence dislocations in compounds of this type may be not only of the sessile type, although the destruction pattern is often of the brittle (cleavage) type.

Note that the microhardness of film I (see table, reduced values of H_0), displaying typically nonhomogeneous deformation, is considerably higher than that of film IV being deformed homogeneously. The difference in the hardness of hexagonal films (I and II) obtained under different conditions of magnetron synthesis, which was also observed by other authors (see [15]), remains unclear.

Thus, the high-resolution transmission and scanning electron microscopy revealed that amorphous inclusions and interlayers at the boundaries between crystallites are absent for most nanostructured nitride–boride films under investigation and the boundaries have a predominantly crystalline structure. For film III, with a crystallite size 0.5–3 nm, the situation remains unclear and requires further investigation. The presence of intracrystallite edge dislocations is confirmed by estimates obtained in [16, 17]. The deformation under indentation of films can be of a homogeneous or a nonhomogeneous, localized type, which is hypothetically attributed to the difference in the behavior of the columnar structure of the films. The proposed possibility of plastic deformation of "columns" of TiN correlates with the presence of intracrystallite dislocations revealed experimentally.

ACKNOWLEDGMENTS

The authors are grateful to A.S. Aronin, A.M. Glezer, N.I. Noskova, and R.Z. Valiev for fruitful discussions of the results and to K. Ma (Taiwan) and D. Hull (Great Britain) for their assistance in fractographic and Auger experiments. We are also grateful to the Departments of Materials Science at the Universities of Ehime (Japan), and Birmingham and Loughborough (Great Britain) for letting us use their equipment.

This research was carried out under the support of INTAS program (project no. 96-2232) and "Integration" program (project no. 855).

REFERENCES

1. R. A. Andrievskiĭ, G. V. Kalinnikov, N. P. Kobelev, *et al.*, Fiz. Tverd. Tela (S.-Peterburg) **39**, 1859 (1997) [Phys. Solid State **39**, 1661 (1997)].
2. J.-E. Sundgren and L. Hultman, in *Materials and Processes for Surface and Interface Engineering*, Ed. by Y. Pauleau (Kluwer, Dordrecht, 1995), p. 453.
3. M. Shiwa, E. Wepelmann, D. Munz, *et al.*, J. Mater. Sci. **31**, 5985 (1996).
4. J. P. Riviere, Ph. Guesdon, J. Delafond, *et al.*, Thin Solid Films **204**, 151 (1991).
5. H. Deng, J. Chen, R. B. Inturi, *et al.*, Surf. Coat. Technology **76–77**, 609 (1995).
6. X. Wang, P. J. Martin, and T. J. Kinder, Surf. Coat. Technology **78**, 37 (1996).
7. R. Wiedemann, H. Oettel, and M. Jerenz, Surf. Coat. Technology **97**, 313 (1997).
8. K. Ma, A. Bloyce, R. A. Andrievskiĭ, *et al.*, Surf. Coat. Technology **94–95**, 322 (1997).
9. R. A. Andrievskiĭ, J. Solid State Chem. **133**, 249 (1997).
10. E. Kelesoglu and C. Mitterer, Surf. Coat. Technology **98**, 1483 (1998).
11. R. A. Andrievskiĭ, in *Surface-Controlled Nanoscale Materials for High-Added-Value Application*, Ed. by K. E. Gonsalves, M.-I. Baraton, R. Singh, *et al.* (Mater. Res. Soc., Warrendale, 1998), **501**, p. 149.
12. R. A. Andrievskiĭ, Usp. Khim. **66**, 57 (1997).
13. B. Jonsson and S. Hogmark, Thin Solid Films **114**, 257 (1984).
14. R. A. Andrievskiĭ, Materialovedenie No. 8 (1999) (in press).
15. R. A. Andrievskiĭ, Usp. Khim. **63**, 431 (1994).
16. V. G. Gryaznov, A. M. Kaprelov, and A. E. Romanov, Pis'ma Zh. Tekh. Fiz. **15** (2), 55 (1989) [Sov. Tech. Phys. Lett. **15**, 39 (1989)].
17. V. G. Gryaznov, I. A. Polonsky, A. E. Romanov, *et al.*, Phys. Rev. B **44**, 42 (1991).
18. M. Odén, H. Ljungcrantz, and L. Hultman, J. Mater. Res. **12**, 2134 (1997).

19. R. A. Andrievskiĭ and I. I. Spivak, *Strength of Refractory Compounds and Materials on Their Basis* (Metallurgiya, Chelyabinsk, 1989).
20. A. M. Glezer and B. V. Molotilov, *Structure and Mechanical Properties of Amorphous Alloys* (Metallurgiya, Moscow, 1992).
21. V. I. Al'shits and G. V. Berezhkova, in *Physical Crystallography* (Nauka, Moscow, 1992) [Phys. Solid State **39** (1995)].
22. N. P. Skvortsova, Fiz. Tverd. Tela (S.-Peterburg) **37**, 3347 (1995).
23. G. Spathis, J. Mater. Sci. **32**, 1943 (1997).
24. D. S. Yan, Y. S. Zheng, and L. Gao, J. Mater. Sci. **33**, 2719 (1998).
25. J. E. Garsley, A. Fisher, W. W. Milligan, *et al.*, Metall. Mater. Trans. A **29**, 2261 (1998).
26. T. R. Malow and C. C. Koch, Metall. Mater. Trans. A **29**, 2285 (1998).
27. K. J. Ma and A. Bloyce, Surf. Eng. **11**, 71 (1995).
28. R. A. Andrievskiĭ, in *Nanostructured Materials: Science and Technology*, Ed. by G.-M. Chow and N. I. Noskova (Kluwer, Dordrecht, 1998), p. 263.
29. R. Yamamoto, S. Murakami, and K. Maruyama, J. Mater. Sci. **33**, 2047 (1998).

Translated by N. Wadhwa